The Cerebellum (2020) 19:510–526
https://doi.org/10.1007/s12311-020-01125-7

ORIGINAL PAPER

Nitric Oxide Critically Regulates Purkinje Neuron Dendritic Development Through a Metabotropic Glutamate Receptor Type 1–Mediated Mechanism

Vasiliki Tellios[1,2] · Matthew J. E. Maksoud[1,2] · Yun-Yan Xiang[2] · Wei-Yang Lu[1,2,3]

Published online: 8 April 2020

Abstract

Nitric oxide (NO), specifically derived from neuronal nitric oxide synthase (nNOS), is a well-established regulator of synaptic transmission in Purkinje neurons (PNs), governing fundamental processes such as motor learning and coordination. Previous phenotypic analyses showed similar cerebellar structures between neuronal nitric oxide null ($nNOS^{-/-}$) and wild-type (WT) adult male mice, despite prominent ataxic behavior within $nNOS^{-/-}$ mice. However, a study has yet to characterize PN molecular structure and their excitatory inputs during development in $nNOS^{-/-}$ mice. This study is the first to explore morphological abnormalities within the cerebellum of $nNOS^{-/-}$ mice, using immunohistochemistry and immunoblotting. This study sought to examine PN dendritic morphology and the expression of metabotropic glutamate receptor type 1 (mGluR1), vesicular glutamate transporter type 1 and 2 (vGluT1 and vGluT2), stromal interaction molecule 1 (STIM1), and calpain-1 within PNs of WT and $nNOS^{-/-}$ mice at postnatal day 7 (PD7), 2 weeks (2W), and 7 weeks (7W) of age. Results showed a decrease in PN dendritic branching at PD7 in $nNOS^{-/-}$ cerebella, while aberrant dendritic spine formation was noted in adult ages. Total protein expression of mGluR1 was decreased in $nNOS^{-/-}$ cerebella across development, while vGluT2, STIM1, and calpain-1 were significantly increased. Ex vivo treatment of WT slices with NOS inhibitor L-NAME increased calpain-1 expression, whereas treating $nNOS^{-/-}$ cerebellar slices with NO donor NOC-18 decreased calpain-1. Moreover, mGluR1 agonist DHPG increased calpain-1 in WT, but not in $nNOS^{-/-}$ slices. Together, these results indicate a novel role for nNOS/NO signaling in PN development, particularly by regulating an mGluR1-initiated calcium signaling mechanism.

Keywords Nitric oxide · Purkinje neuron · Development · Metabotropic glutamate receptors

Introduction

Mutant mice have been crucial in discerning key pathways associated with cerebellar development and pathogenesis. Although many have been identified and characterized in terms of cerebellar morphology, a number of mutant mice that exhibit ataxic behaviors have yet to be characterized at the molecular level. A well-known modulator of synaptic transmission and function within the cerebellum is nitric oxide (NO), produced primarily by neuronal nitric oxide synthase (nNOS). The cerebellar cortex expresses the highest levels of nNOS, and therefore produces higher concentrations of NO than any other region of the brain [1]. In addition, NO is known to play a crucial role in the modulation of the long-term depression (LTD) profile of cerebellar Purkinje neurons (PNs), responsible for encoding motor learning and coordination across development [2]. Moreover, a study characterizing the expression level and functionality of nNOS/NO production noted a significant downregulation in nNOS mRNA and activity in cerebellar mutant mice, including *leaner*, *staggerer*, *nervous*, and *Purkinje cell degeneration* mice [3]. Accordingly, in vivo deletion of nNOS in mice ($nNOS^{-/-}$) results in an ataxic phenotype with significant motor impairments and tremors [4–6]. Despite these already established

Electronic supplementary material The online version of this article (https://doi.org/10.1007/s12311-020-01125-7) contains supplementary material, which is available to authorized users.

✉ Wei-Yang Lu
wlu53@uwo.ca

[1] Graduate Program of Neuroscience, The University of Western Ontario, London N6A 5B7, Canada

[2] Robarts Research Institute, London N6A 5B7, Canada

[3] Department of Physiology and Pharmacology, The University of Western Ontario, London N6A 5B7, Canada

behavioral deficits, preliminary gross anatomical analyses of the adult nNOS$^{-/-}$ mouse brain revealed no noticeable abnormalities in cerebellar morphology, which included length of dendritic arborization and overall cerebellar volume [6].

Under physiological conditions, endogenous NO signaling regulates calcium influx into PNs by modulating excitatory parallel fiber (PF) and climbing fiber (CF) inputs. Both PF and CF inputs determine the LTD profile of the PN [7]. Calcium influx and efflux is heavily regulated within the physiological PN, and chronic increases in cytosolic calcium concentrations have been reported to cause a number of cerebellar pathologies, including a variety of spinocerebellar ataxias (SCAs) as well as severe cognitive delays [8–10]. Specifically, activation of metabotropic glutamate receptor type 1 (mGluR1), localized on dendritic spines of PNs, stimulates the production of inositol triphosphate (IP3) via phospholipase-C (PLC) activity [11, 12]. IP3 then binds to its endogenous receptor on the endoplasmic reticulum (ER), resulting in calcium efflux from the ER to the cytosol [13]. The low concentration of calcium in the ER causes stromal interaction molecule 1 (STIM1) oligomerization and transient receptor potential canonical type 3 (TRPC3) channel activity, mediating store operated calcium entry [14–17]. Importantly, a recent paper explained the crucial interaction between STIM1 and NO, which functions to prevent the influx of calcium through store-operated mechanisms [18].

Although both ionotropic and metabotropic glutamate receptors are important for the facilitation of calcium entry into the PN, many studies have noted the importance of mGluRs, specifically mGluR1, in the development of cerebellar pathologies and ataxias. For example, overactivation of mGluR1 in an SCA1 mouse model led to decreased PN dendritic branching [19]. Conversely, decreased expression of mGluR1 on PNs has led to deficits, specifically related to LTD [20]. Particularly within human SCAs, a variety of genes associated with the mGluR1 pathway are mutated that can cause symptoms such as tremor, loss of balance, and fine movement control. For example, the genes *ITPR1*, *TRPC3*, and *GRM1* encoding IP3R, TRPC3, and mGluR1 are affected in SCA15, SCA41, and SCA44, respectively, resulting in altered calcium influx within the PN [21–23].

Considering the importance of nNOS/NO signaling in the physiological development of the cerebellum [4] and the lack of characterization of PN development in the absence of nNOS/NO signaling [6], this study sought to examine general morphological differences in PN dendritic structures across postnatal development between wild-type (WT) and nNOS$^{-/-}$ mice. Specifically, the present study aimed to delineate potential structural changes in dendrite and synapse phenotype in nNOS$^{-/-}$ cerebella, alterations in synaptic proteins associated with the mGluR1 pathway, and a potential mechanism in which NO may influence dendritic morphology.

Materials and Methods

Animals

WT (C57BL/6J, Stock No. 000664) and nNOS$^{-/-}$ mice (B6.129S4-Nos1^{tm1Plh}, Stock No. 002986) were purchased from the Jackson Laboratory. All experiments were conducted in accordance with Animal Use Protocol (#2018-106) approved by the Animal Care and Veterinary Services at the University of Western Ontario. Timepoints for cerebellar collection occurred at postnatal day 7 (PD7), 2 weeks (2W), and 7 weeks (7W) of age on male mice.

Immunohistochemical Preparation

Whole brains were isolated from WT and nNOS$^{-/-}$ mice and immediately placed in 4% paraformaldehyde (PFA) for 48 h. Brains were subsequently transferred to a 30% sucrose solution for at least 48 h. Brains were sagittally sectioned at a thickness of 40 μm using a vibratome, placed in a cryoprotectant solution, and stored in − 20 °C until stained. Slices were first washed with PBS, then permeabilized using a 0.25% Triton-X solution for 5 min. Slices were then blocked with a 10% normal donkey serum (NDS) solution for 1 h and incubation with the following primary antibodies overnight in 4 °C: 1:500 goat anti-calbindin (CalB) (Santa Cruz Biotechnology, Dallas, TX), 1:800 rabbit anti-mGluR1 (Novus Biologicals, Oakville, ON), 1:500 guinea pig anti-vesicular glutamate transporter type 1 (vGluT1), 1:500 guinea pig anti-vesicular glutamate transporter type 2 (vGluT2) (Synaptic Systems, Goettingen, Germany), 1:200 rabbit anti-STIM1 (Proteintech Group Inc., Rosemont, IL), or 1:500 rabbit anti-calpain-1 (Abcam, Toronto, ON). Slices were washed and then incubated with the appropriate secondary antibodies for 2 h: anti-rabbit Cy3, anti-goat AlexaFluor 488, or anti-guinea pig AlexaFluor 488 (Jackson Immunoresearch, Burlington, ON). Slices were mounted on cover glass using Fluoromount-G (Electron Microscopy Solutions, Hatfield, PA), and images were taken using the Olympus FV1000 confocal microscope at ×60 magnification using an oil immersion objective.

Western Blotting

Total Protein Isolation

Cerebella were isolated from WT and nNOS$^{-/-}$ mice and stored at − 80 °C. Cerebellar lysates were obtained by homogenizing the cerebellar tissues using a glass homogenizer in radioimmunoprecipitation assay (RIPA) lysis buffer, supplemented with 0.1% apoprotein and 0.1% leupeptin. Once homogenized, lysates were centrifuged for 30 min at 4 °C. The supernatant was collected, and protein was measured using a Bradford reagent mix (Bio-Rad, Hercules, CA).

Plasma Membrane Protein Isolation

Plasma membrane protein fractions were isolated using the commercially available Mem-PER Plus Membrane Protein Extraction Kit (ThermoFisher Scientific, Rockford, USA) following the manufacturer's instructions.

Samples were later prepared using ×2 sample buffer and loaded onto 8% or 10% polyacrylamide gels for electrophoresis and run for 2 h at 100 V. Gels were then wet transferred onto nitrocellulose membranes for 2 h at 80 V. Blots were blocked in 5% bovine serum albumin (BSA) for 1 h before incubation with the following primary antibodies overnight: 1:800 rabbit anti-mGluR1 (142 kDa), 1:500 guinea pig anti-vGluT1 (62 kDa), 1:800 rabbit anti-STIM1 (90 kDa), 1:500 guinea pig anti-vGluT2 (64 kDa), 1:500 rabbit anti-β-III-spectrin (270 kDa) (Proteintech Group Inc., Rosemont, IL), 1:500 mouse anti-calpain-1 (80 kDa) (Santa Cruz Biotechnology, Dallas, TX), 1:200 guinea pig anti-GluR1 (AMPA subunit, 100 kDa), or 1:10,000 anti-glyceraldehyde-3-phosphate dehydrogenase (GAPDH, 40 kDa) (Abcam, Toronto, ON) for total protein comparisons, and sodium/potassium adenosine triphosphatase (Na^+/K^+ ATPase, 100 kDa) (Abcam, Toronto, ON) for plasma membrane protein comparisons. After three washes in tris-buffered saline solution, the appropriate secondary horseradish-peroxidase antibodies (Jackson Immunoresearch, Burlington, ON) were incubated on the membranes for 1.5 h. Protein was visualized using enhanced chemiluminescence substrate (Bio-Rad, Hercules, CA) and imaged using the Bio-Rad VersaDoc system. All proteins were normalized to the housekeeping protein GAPDH or Na^+/K^+ ATPase. Densitometric analyses were quantified using FIJI open source software.

Ex Vivo Organotypic Cerebellar Slice Cultures

Cerebella were obtained from 10 to 12 postnatal day (PD) 0 WT and $nNOS^{-/-}$ pups and dissected in Hank's balanced salt solution (HBSS) containing 15 mM 4-(2-hydroxyehtyl)-1-piperazineethanesulfonic acid (HEPES), 0.5% glucose, and 2% sucrose and maintained at pH 7.3 and 315 mOsm. Once isolated, the cerebella were sliced at a thickness of 350 μm using a tissue chopper and carefully isolated and plated on 35-mm membrane inserts (Milipore Ltd., Etobicoke, ON). The bottom half of the insert was exposed to cerebellar slice culture media containing minimum essential medium (MEM) supplemented with 5 mg/ml glucose, 25% heat-inactivated horse serum, 25 mM HEPES, 1 mM glutamine, and 100 U/ml penicillin and streptomycin. Slice cultures were maintained for 7 days in vitro (DIV7), and half of the medium was refreshed every 2 days. WT slice cultures were treated with either NOS inhibitor N(G)-nitro-L-arginine methyl ester (L-NAME, 100 μM) (Santa Cruz Biotechnology, Dallas, TX), mGluR1 agonist dihydroxyphenylglycine (DHPG, 10 μM), and mGluR1 antagonist LY367385 (10 μM) (Tocris Bioscience, Oakville, ON). $nNOS^{-/-}$ cultures were treated with a slow NO donor, diethylenetriamine NONOate (NOC-18, 300 μM) (Santa Cruz Biotechnology, Dallas, TX). Cultured cerebellar slices were either used for western blotting or immunohistochemistry.

Ex Vivo Slice Culture Immunohistochemistry

Organotypic cerebellar slice cultures were established and maintained as previously described. Once slices reached DIV7, slices were incubated in 4% PFA solution for 2 h at 4 °C, washed with PBS, and later left to permeabilize in 0.25% Triton-X solution for 4 h. Slices were then left in 5% NDS blocking solution for 2 h before addition of primary anti-goat CalB (1:500) overnight. Secondary antibodies were incubated for 2 h, and slides were mounted. Images were taken using the Olympus FV1000 confocal microscope and a ×60 oil immersion objective.

Image Analysis

Strahler Analysis

PD7 PN dendrites were analyzed using the Strahler analysis plugin available on FIJI opensource software [24]. Briefly, confocal images labeled with CalB were made binary, thresholded, and skeletonized. Each PN was analyzed separately, and all parameters remained consistent across WT and $nNOS^{-/-}$ images. Individual PN somata were identified for each image, and the Strahler analysis plugin was used to identify the total number of dendritic branches per cell. Total branch number per cell was averaged from multiple images across four biological replicates.

Dendritic Thickness

Dendritic thickness reports the diameter of the largest primary, aspinous dendrites per confocal image representing CalB from 7W WT and $nNOS^{-/-}$ mice using FIJI. Briefly, the five largest branches were identified per image and measured in micrometers (μm) using the straight line tool. Dendritic thickness was averaged from multiple images across four biological replicates.

Spine Morphology

Spine morphology and characterization was determined using NeuronStudio. Briefly, spine head, neck, and length of spine parameters were set using the default settings, which remained unchanged between WT and $nNOS^{-/-}$ images. The spine classification tool would use the head-to-neck diameter ratio as well as the length of the spine to classify each spine as either

mushroom, thin or stubby. The number of mushroom, thin or stubby spine type, was averaged across multiple dendritic branches of 10 μm in length over four biological replicates.

Particle Tracking

The number of PN dendritic spines as well as mGluR1, STIM1, and vGluT2 clusters were determined using the Particle Tracker 2D/3D plugin available on FIJI. Parameters for the radius of particle detection, the non-particle discrimination cutoff, and absolute intensity values remained consistent across WT and nNOS$^{-/-}$ samples for each target protein analyzed. The total number of PN dendritic spines and mGluR1 clusters were determined within non-overlapping ROIs of 300 × 300 μm located specifically within the distal dendritic region of the molecular layer (top 50% of the dendritic area) and averaged across multiple images over four biological replicates. The average number of STIM1 clusters within each PN soma was determined using the image analysis method highlighted in Figure S1. The localization and number of vGluT2 clusters for both WT and nNOS$^{-/-}$ cerebella were determined using the Particle Tracker 2D/3D, as shown in Figure S2.

Integrated Density Analysis

Calpain-1 fluorescence intensity within PN somata of 7W WT and nNOS$^{-/-}$ cerebella was measured using FIJI. Briefly, an ROI of the PN soma, determined using the CalB stain, was made and overlayed on the corresponding calpain-1 image. Then, integrated density—measured in arbitrary units of intensity (AUIs)—was graphed for each WT and nNOS$^{-/-}$ PN soma. Integrated density was averaged from multiple cells across four biological replicates.

Statistical Analysis

Statistical analyses were performed using an unpaired, two-tailed *t* test for all results comparing WT to nNOS$^{-/-}$ mice. Results obtained from organotypic slice cultures were analyzed using a one-way ANOVA corrected with a Tukey's post hoc test. Significance was determined using a threshold of $P = 0.05$. All values were reported as mean ± standard error of the mean (SEM).

Results

PN Dendritic Branching and Spine Density Are Reduced in the Cerebella of Young and Adult nNOS$^{-/-}$ Mice

We first investigated whether nNOS$^{-/-}$ mice displayed alterations in PN morphology during early postnatal development. Despite previous gross anatomical analyses showing no obvious structural changes in the cerebellum of adult nNOS$^{-/-}$ mice [6], confocal images of PD7 cerebella showed dramatically less dendritic branching ubiquitously across all PNs in nNOS$^{-/-}$ mice compared with age-matched WT controls (Fig. 1a), while the total number of PN cell somata remained the same between WT and nNOS$^{-/-}$ mice (Fig. 1b). In accordance with this trend, a Strahler analysis quantifying the number of terminal branches per PN showed a significantly lower number of terminal branches for individual PNs of nNOS$^{-/-}$ mice compared with WT (Fig. 1c, d).

We next investigated whether the alteration in nNOS$^{-/-}$ PN morphology carried on into adulthood. Confocal images displaying CalB-immunoreactive PN structures showed dramatically different PN branching between WT and nNOS$^{-/-}$ mice (Fig. 2a), while image analyses revealed no significant difference in soma number or PN dendritic length in nNOS$^{-/-}$ mice compared with WT at 7W (Fig. 2b, c). However, primary aspiny PN dendrites in nNOS$^{-/-}$ cerebella were significantly thicker compared with WT mice (Fig. 2d). Additionally, PN dendritic spine morphology was significantly affected in nNOS$^{-/-}$ mice. Specifically, analysis of spine type determined a significant shift from predominantly mushroom-type spines found on WT PNs to predominantly thin-type spines found on nNOS$^{-/-}$ PNs (Fig. 2e–g), while stubby spines remained unchanged between WT and nNOS$^{-/-}$ (data not shown). In general, the overall number of spines on PN dendrites was significantly less in nNOS$^{-/-}$ mice compared with WT controls (Fig. 2h).

mGluR1 Expression Is Reduced in the Cerebella of Young and Adult nNOS$^{-/-}$ Mice

We also characterized the postsynaptic component of glutamatergic synapses, first with a focus on mGluR1 protein expression. Immunohistochemistry revealed that immunofluorescent clusters of mGluR1 in the cerebella of PD7 mice were primarily located on the tip of PN dendritic spines, while some mGluR1 clusters were localized to the PN soma. Notably, overall mGluR1 expression levels were significantly lower in PD7 nNOS$^{-/-}$ cerebella compared with age-matched WT mice (Fig. 3a, b). The observed decrease in mGluR1 protein expression in PD7 nNOS$^{-/-}$ cerebella was consistent at 2W, as determined using western blot (Fig. 3c, d).

Again, nNOS$^{-/-}$ cerebella continued to express lower levels of mGluR1 at 7W (Fig. 4). Specifically, the number of mGluR1 clusters was significantly less in nNOS$^{-/-}$ cerebella (Fig. 4a, b), and total expression levels of mGluR1 were significantly lower in nNOS$^{-/-}$ cerebella at 7W, determined by western blot (Fig. 4c). Interestingly, the plasma membrane (PM) expression of mGluR1 in cerebellar samples revealed significantly more mGluR1 expression on the membrane in nNOS$^{-/-}$ mice compared with WT at 7W (Fig. 4d). To ensure

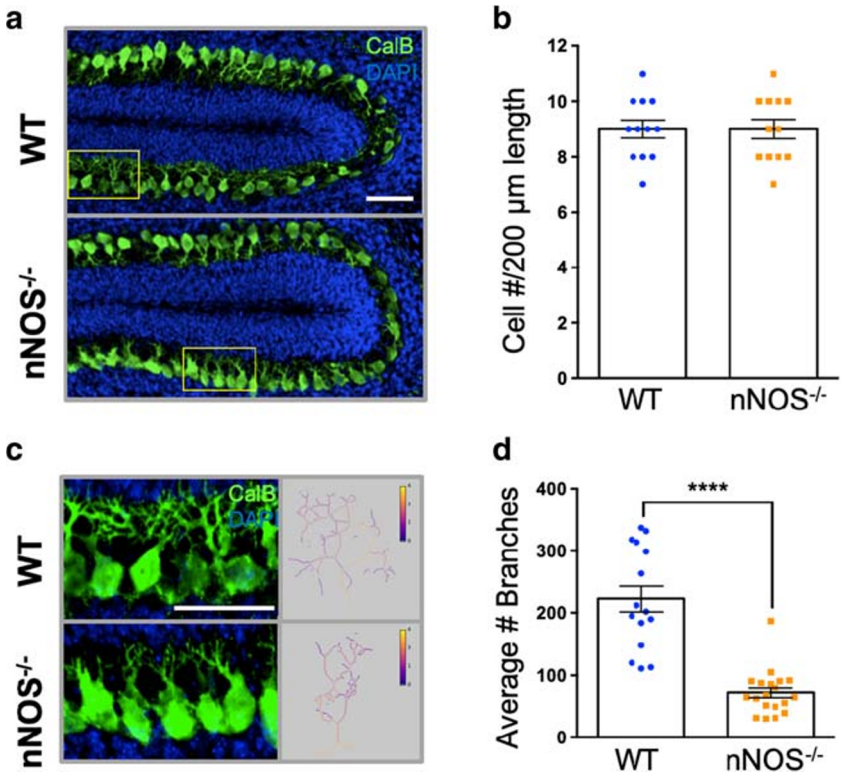

Fig. 1 PN dendritic branching is robustly altered in PD7 nNOS$^{-/-}$ cerebella. **a** Representative confocal images of WT and nNOS$^{-/-}$ PNs expressing CalB (green) and nuclei stained by DAPI (blue). Scale bars represent 100 μm. **b** Bar graph represents the number of PN cell somata per 200 μm length. $N = 4$ biological replicates per group; WT $n = 12$ cells, nNOS$^{-/-}$ $n = 12$ cells. $P = 0.99$. **c** Enlarged representation of WT and nNOS$^{-/-}$ PNs and subsequent Strahler analysis profile, indicating degrees of branching and branch number. Scale bar represents 50 μm. **d** Bar graph represents average number of PN branches as determined using a Strahler analysis. $N = 4$ biological replicates per group; WT $n = 15$ cells, nNOS$^{-/-}$ $n = 19$ cells. $P < 0.0001$. All data are represented as mean ± SEM

that the mGluR1 pathway in particular is affected, PM expression of the GluR1 subunit of AMPARs, the main ionotropic glutamate receptor on PNs, was assayed using western blot, and no significant differences were noted between WT and nNOS$^{-/-}$ mice at 7W (Fig. 4e).

vGluT1 Expression Is Reduced in PD7 nNOS$^{-/-}$ Cerebella, but Not at 2W or 7W

To determine whether alterations also occurred in the presynaptic compartment of PF-PN synapses in nNOS$^{-/-}$ mice, PF terminals were selectively labeled with vGluT1 and analyzed using confocal microscopy. At PD7, vGluT1 expression was significantly lower in nNOS$^{-/-}$ cerebella, as determined by western blot (Fig. 5a, b). By 2W, this difference was no longer noticeable (Fig. 5c), and western blotting at this time point showed no significant difference in protein levels between nNOS$^{-/-}$ and age-matched WT controls (Fig. 5d). This same trend was noticed at 7W, where immunohistochemical staining and western blots did not reveal a significant difference in vGluT1 expression (Fig. 5e, f).

vGluT2 Expression Is Increased in 7W nNOS$^{-/-}$ Cerebella

Considering another crucial glutamatergic synapse on PNs arises from climbing fiber (CF) innervation, we immunostained vGluT2—a specific marker for CF boutons—to determine whether the CF-PN synapse is affected in nNOS$^{-/-}$ mice. Western blots using cerebellar tissue from WT and nNOS$^{-/-}$ PD7 and 2W mice revealed no significant difference in vGluT2 expression (Fig. 6a, b). However, immunoblots of 7W cerebella revealed a nearly two-fold increase in vGluT2 expression in nNOS$^{-/-}$ mice compared with WT (Fig. 6c). Interestingly, further analysis of fluorescently labeled vGluT2 in 7W nNOS$^{-/-}$ cerebella revealed more vGluT2 clusters within the upper 20% area, closest to the pial surface (Fig. 6d, e). A significant difference in clustering was not noted in the lower 80% of the molecular layer (Fig. 6f), and no significant differences in vGluT2 staining within the granule cell layer (denoting mossy fiber innervation) were detected (data not shown).

STIM1 Expression and Cluster Density Is Increased in nNOS$^{-/-}$ Cerebella

The specific alterations in mGluR1 expression in nNOS$^{-/-}$ cerebella led us to investigate whether localization and expression of STIM1, an ER calcium sensor implicated downstream of mGluR1 signaling [15], was changed in the PNs of nNOS$^{-/-}$ mice. Immunohistochemistry showed that at PD7, STIM1 immunoreactive clustering was significantly more abundant within the PN soma of nNOS$^{-/-}$ mice compared with PNs of WT mice at this time point (Fig. 7a, b). In addition, a higher level of STIM1 protein expression in nNOS$^{-/-}$ cerebella was determined by western blot at PD7 (Fig. 7c).

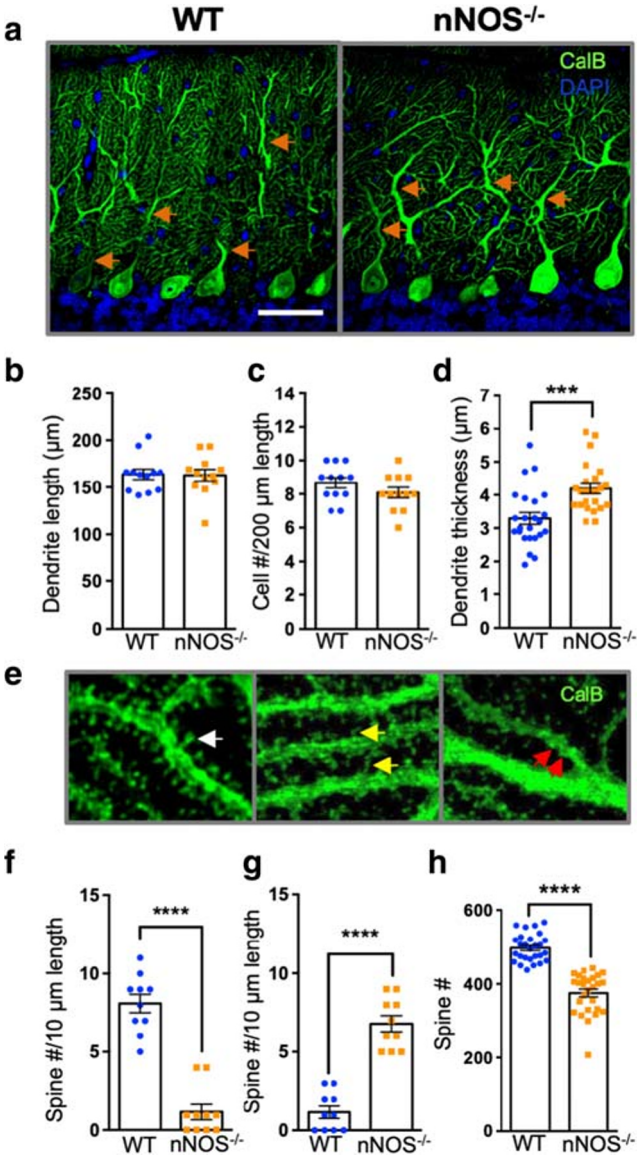

Fig. 2 Alterations in PN dendritic branching and synapse morphology in nNOS$^{-/-}$ cerebella at 7W. **a** Representative confocal images of WT and nNOS$^{-/-}$ PNs using CalB (green) at 7W. Orange arrows depict aspinous primary branches. Scale bar represents 50 μm. **b** Bar graph represents length of dendrites, from PN cell soma to pial surface. $N = 4$ biological replicates per group; WT $n = 12$ images, nNOS$^{-/-}$ $n = 12$ images. $P = 0.9028$. **c** Bar graph represents number of PN cell somata per 200-μm length. $N = 4$ biological replicates per group; WT $n = 12$ images, nNOS$^{-/-}$ $n = 12$ images. $P = 0.1988$. **d** Bar graph represents average thickness of primary aspinous dendrites. $N = 4$ biological replicates per group; WT $n = 25$ branches, nNOS$^{-/-}$ $n = 25$ branches. $P = 0.0003$. **e** Representative confocal images of mushroom spines (white arrows), thin spines (yellow arrows), and stubby spines (red arrows). Classification of spine morphology was performed using NeuronStudio. **f** Bar graph represents number of mushroom spines between WT and nNOS$^{-/-}$ mice at 7W. $N = 4$ biological replicates per group; WT $n = 10$ images, nNOS$^{-/-}$ $n = 10$ images. $P < 0.0001$. **g** Bar graph represents number of thin spines between WT and nNOS$^{-/-}$ mice at 7W. $N = 4$ biological replicates per group; WT $n = 10$ images, nNOS$^{-/-}$ $n = 10$ images. $P < 0.0001$. **h** Bar graph represents total spine number per 300 × 300 μm ROI between WT and nNOS$^{-/-}$ mice at 7W. $N = 4$; WT $n = 27$, nNOS$^{-/-}$ $n = 27$. $P < 0.0001$. All data are represented as mean ± SEM

STIM1 expression remained elevated in the PNs of nNOS$^{-/-}$ mice at 2W, evidenced by significantly more immunoreactive STIM1 clusters within PN somata (Fig. 7d, e). Additionally, a higher level of STIM1 protein expression in the nNOS$^{-/-}$ cerebellum when compared with WT cerebella was determined by western blot (Fig. 7f).

The elevated STIM1 clustering and expression in the PNs of nNOS$^{-/-}$ mice continued in 7W nNOS$^{-/-}$ cerebella, determined by immunohistochemistry and western blotting (Fig. 7g–i). Elevated STIM1 expression and clustering suggests altered calcium dynamics within the PNs of the nNOS$^{-/-}$ mice.

Increased Calpain-1 Expression Corresponds with a Decrease in β-III-Spectrin in Both Young and Adult nNOS$^{-/-}$ Cerebella

Considering that STIM1 activity is crucial in regulating calcium influx into the PN, we therefore explored the potential consequences of aberrant calcium signaling that could alter PN morphology. Calpains are important calcium-dependent proteases that, when activated, are responsible for the cleavage of proteins involved in neuronal structural integrity [25]. Western blots for calpain-1 at PD7, 2W, and 7W all demonstrated significantly elevated levels of calpain-1 within the cerebella of nNOS$^{-/-}$ mice (Fig. 8a–c). To ensure localization of calpain-1 with PNs specifically, we have also made immunofluorescent stains for calpain-1, which showed global calpain-1 presence, with relatively high expression with PN somata and dendrites in both WT and nNOS$^{-/-}$ cerebella (Fig. 8d). A measurement of calpain-1 integrated density within the PN somata revealed significantly increased calpain-1 expression within nNOS$^{-/-}$ PNs compared with WT at 7W, mirroring the western blot data (Fig. 8e). In accordance with this upregulation of calpain-1, levels of β-III-spectrin, a calpain substrate and an important PN-specific structural protein, were decreased at 7W in nNOS$^{-/-}$ mice compared with age-matched WT controls (Fig. 8f).

NO Signaling Regulates the mGluR1-Dependent Expression of Calpain-1 in nNOS$^{-/-}$ Organotypic Cerebellar Slice Cultures

To determine whether the changes in morphology and protein expression in nNOS$^{-/-}$ PNs were a consequence of a lack of NO signaling within the cerebellum, we established ex vivo organotypic cultures of cerebellar slices and treated the cultured slices with various compounds. Treating WT cerebellar slices with either L-NAME, a NOS inhibitor, or with DHPG, an mGluR1 agonist, seemed to greatly decrease dendritic branching of PNs in cultured slices compared with controls (Fig. 9a). In accordance with the observed detrimental effects on dendritic morphology, L-NAME and DHPG significantly

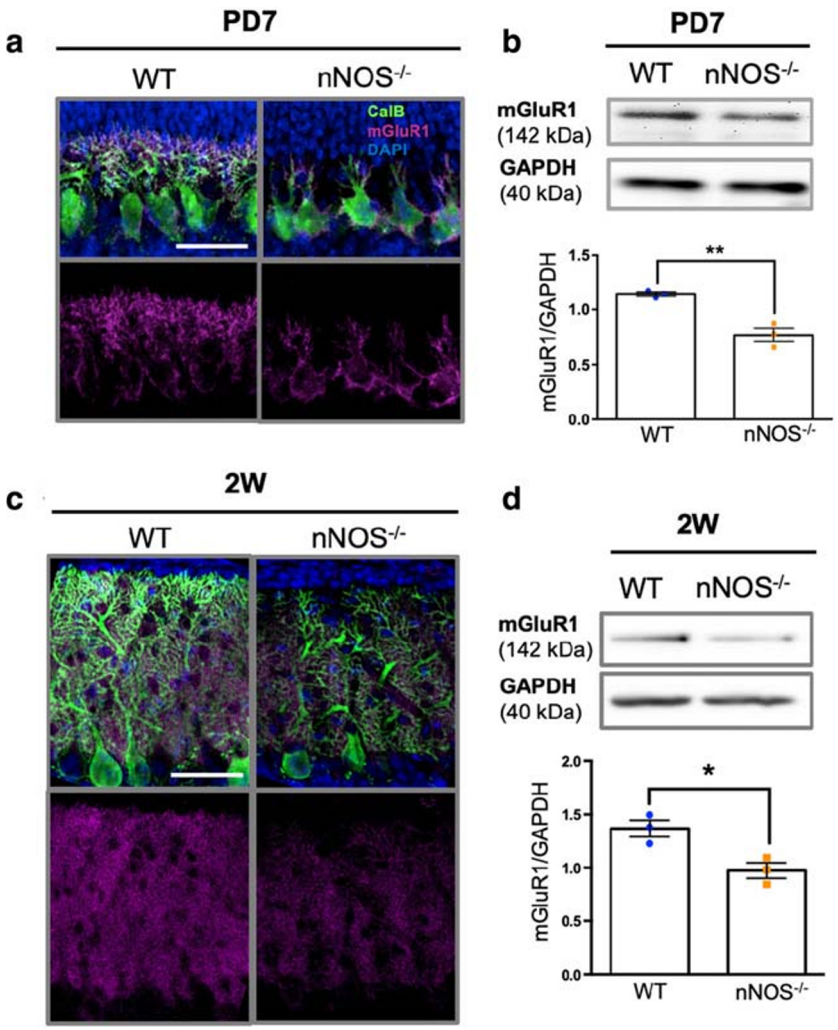

Fig. 3 mGluR1 expression is decreased in nNOS$^{-/-}$ PNs at PD7 and 2W. **a** Representative confocal images of WT and nNOS$^{-/-}$ cerebella stained with CalB (green), DAPI (blue), and mGluR1 (magenta) at PD7. Scale bar represents 50 μm. **b** Representative western blot of total mGluR1 (142 kDa) protein expression for PD7 WT and nNOS$^{-/-}$ cerebella, along with bar graph representing $N = 3$ biological replicates per group. All mGluR1 bands were normalized to GAPDH (40 kDa) expression. $P = 0.0046$. **c** Representative confocal images of WT and nNOS$^{-/-}$ cerebella stained with CalB (green), mGluR1 (magenta), and DAPI (blue) at 2W. Scale bar represents 50 μm. **d** Representative western blot of total mGluR1 protein expression for 2W WT and nNOS$^{-/-}$ cerebella, along with bar graph representing $N = 3$ biological replicates per group. All mGluR1 bands were normalized to GAPDH expression. $P = 0.0211$. All data are represented as mean ± SEM

increased the level of calpain-1 protein expression in WT slices when compared with their controls (Fig. 9a). In contrast, treating WT slices with LY367385, an mGluR1 antagonist, did not seem to alter the dendritic morphology nor the level of calpain-1 expression in comparison with the control (Fig. 9a).

Likewise, organotypic cultures of nNOS$^{-/-}$ slices were treated with either the slow release NO donor NOC-18, DHPG, or LY367385. Notably, NOC-18 treatment seemed to increase dendritic branching while significantly decreasing calpain-1 expression compared with the control (Fig. 9b). Interestingly, DHPG treatment had no effect on calpain-1 levels, while LY367385 treatment seemed to increase dendritic branching while significantly decreasing calpain-1 expression when compared with controls (Fig. 9b).

Discussion

Although the nNOS$^{-/-}$ mouse model experiences behavioral deficits associated with movement coordination and balance [4, 5], a general morphological characterization of the principle cerebellar neurons generating motor output responses had not been fully conducted in this mouse strain. The present study is the first to report distinct alterations in PN morphology of nNOS$^{-/-}$ mice from early postnatal ages to adult. Specifically, our analyses showed that the morphological differences in dendritic branching were accompanied with decreased total mGluR1 expression, along with increased STIM1 expression, and vGluT2 expression only at 7W. Importantly, these changes were associated with increased calpain-1 protein expression in nNOS$^{-/-}$ mice, suggesting aberrant pathway activity and calcium influx. Additionally, modulation of NO as well as mGluR1 signaling affected both PN dendritic branching and calpain-1 expression levels in an ex vivo model.

Dendritic Abnormalities Are Present Within the PNs of nNOS$^{-/-}$ Mice

One of the significant discoveries found by this study is the decrease in PN dendritic branching in nNOS$^{-/-}$ mice from

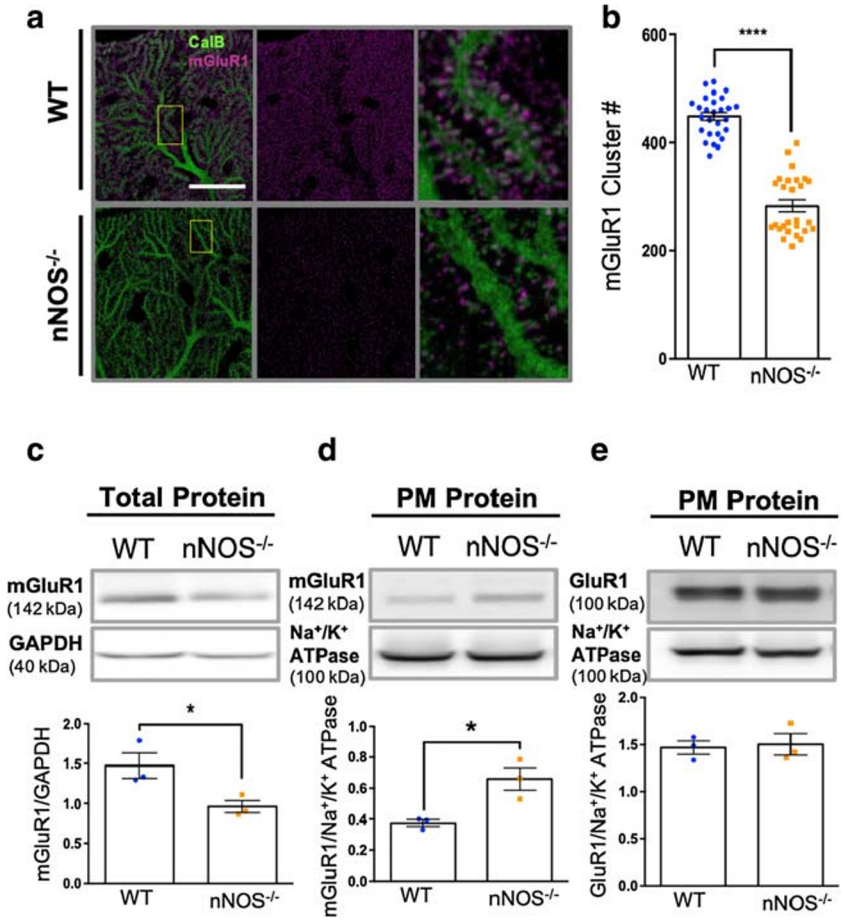

Fig. 4 Total mGluR1 expression is decreased, but PM mGluR1 is increased in the PNs of nNOS$^{-/-}$ at 7W. **a** Representative confocal images of WT and nNOS$^{-/-}$ cerebella stained with CalB (green) and mGluR1 (magenta) at 7W. Images in the right panel are magnified insets of the left panel (area depicted with a yellow box). Scale bar represents 25 μm. **b** Bar graph reports number of mGluR1 clusters per 300 × 300 μm ROI between WT and nNOS$^{-/-}$ cerebella. $N = 4$ biological replicates per treatment; WT $n = 27$ images, nNOS$^{-/-}$ $n = 27$ images. $P < 0.0001$. **c** Representative western blot of total mGluR1 protein expression (142 kDa) for 7W WT and nNOS$^{-/-}$ cerebella, along with bar graph representing $N = 3$ biological replicates per group. Total mGluR1 protein expression was normalized to GAPDH (40 kDa) expression. $P = 0.0434$. **d** Representative western blot of plasma membrane (PM) expression of mGluR1 within WT and nNOS$^{-/-}$ cerebellar tissues at 7W, along with bar graph representing $N = 3$ biological replicates per group. PM mGluR1 protein expression was normalized to Na^+/K^+ ATPase (100 kDa). $P = 0.0205$. **e** Representative western blot of plasma membrane (PM) expression of GluR1 (100 kDa) within WT and nNOS$^{-/-}$ cerebellar tissues at 7W, along with bar graph representing $N = 3$ biological replicates per group. PM GluR1 protein expression was normalized to Na^+/K^+ ATPase. $P = 0.8098$. All data are represented as mean ± SEM

postnatal ages to adulthood. This morphological deficit was expected, considering the importance of NO as a neurotransmitter within the cerebellum [26, 27]. In the cerebellum, NO is produced in an activity-dependent manner from PFs/granule cells and GABAergic interneurons [28], and such activity-dependent NO signaling is essential for the induction of PF-PN synaptic LTD [7, 29, 30], which contributes to spine morphology and calcium regulation within dendrites [31]. While normal neurite growth relies on optimal levels of calcium influx during development, chronically increased calcium suppresses neurite elongation and growth cone movement [32]. Therefore, a lack of NO signaling may affect intracellular calcium transients within the PN and contribute to the dendritic deficits seen in nNOS$^{-/-}$ cerebella during early development.

Altered intracellular calcium signaling within nNOS$^{-/-}$ PNs may also underlie the dramatic shift in dendritic spine type—from mushroom to thin-type spines at 7W. It is reported that mushroom spines are considered "memory spines," harboring features such as larger postsynaptic densities that accommodate more glutamate receptors and better local regulation of calcium influx, leading to functionally stronger synapse formation [33, 34]. In contrast, thin spines or "learning spines" are transient and unstable, harboring smaller postsynaptic densities that either increase in strength or weaken and degrade [34, 35]. Changes from mushroom spines to thin

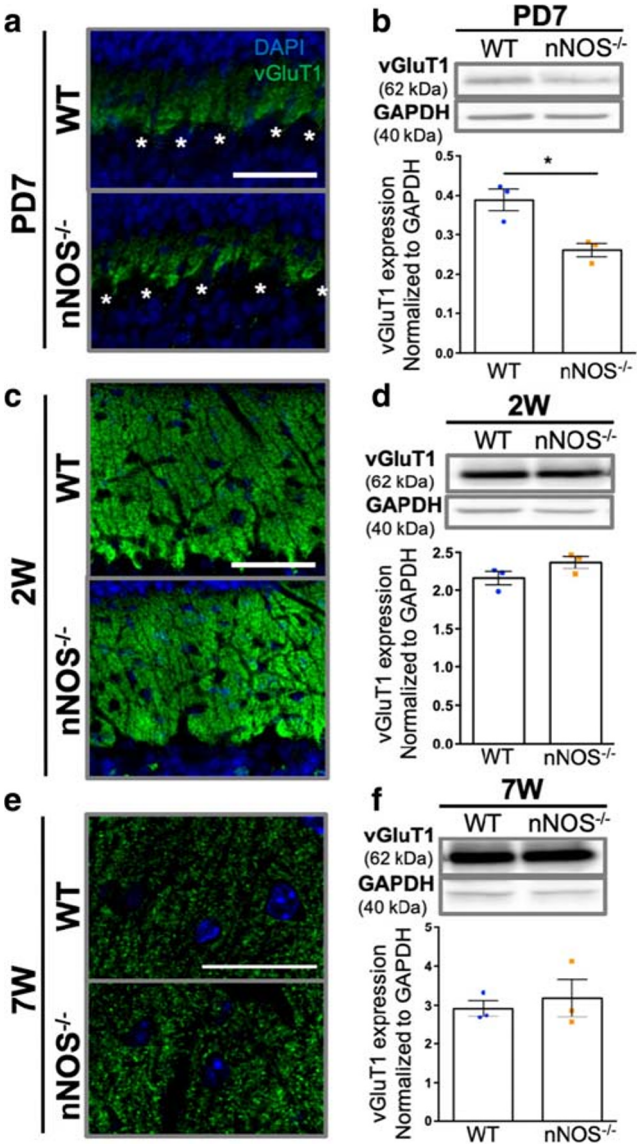

Fig. 5 Expression of vGluT1 is decreased at PD7 in nNOS$^{-/-}$, but this difference is ameliorated by 2W and 7W. **a** Representative confocal images displaying vGluT1 expression (green) and surrounding DAPI (blue) at PD7 in WT and nNOS$^{-/-}$ cerebella. White asterisks represent PN cell somata. Scale bar represents 50 μm. **b** Representative western blot of vGluT1 (62 kDa) protein expression in PD7 WT and nNOS$^{-/-}$ cerebellar tissue. Expression of vGluT1 was normalized to total GAPDH (40 kDa) protein expression. Bar graph represents $N = 3$ biological replicates per group. $P = 0.0179$. **c** Representative confocal images displaying vGluT1 expression (green) and DAPI (blue) at 2W in WT and nNOS$^{-/-}$ cerebella. Scale bar represents 50 μm. **d** Representative western blot of vGluT1 protein expression in 2W WT and nNOS$^{-/-}$ cerebellar tissue. Bar graph represents $N = 3$. $P = 0.6491$. **e** Representative confocal images showing vGluT1 expression (green) and surrounding DAPI (blue) at 7W in WT and nNOS$^{-/-}$ cerebella. Scale bar represents 25 μm. **f** Representative western blot of vGluT1 protein expression in 7W WT and nNOS$^{-/-}$ cerebellar tissue. Bar graph represents $N = 3$ biological replicates per group. $P = 0.6347$. All data are represented as mean ± SEM

spines may rely on the size and time course of calcium dynamics within the nNOS$^{-/-}$ PN, which is an area that warrants investigation in future studies.

Synaptic Alterations Exist Within the PNs of nNOS$^{-/-}$ Mice

Appropriate glutamatergic synapse function is critical in maintaining PN output and motor activity, and this is achieved in part through activation of mGluR1 [36, 37]. Results from this study showed that total mGluR1 protein was significantly decreased in nNOS$^{-/-}$ mice at PD7, 2W, and 7W. Since mGluR1 is predominately located within PN spine heads, decreased total mGluR1 protein expression may be due to decreased dendritic puncta. In addition, decreased PN spine head diameter in nNOS$^{-/-}$ animals can lead to smaller postsynaptic densities and less total synaptic mGluR1 protein accommodation within the PN dendritic spine [38, 39]. It is important to note that PM expression of mGluR1 is indeed higher in nNOS$^{-/-}$ cerebella compared with WT at 7W, while no changes to the GluR1 subunit of the AMPA receptor are seen within this study. The significant increase of mGluR1 on the surface of PNs in nNOS$^{-/-}$ mice might allude to a feedback regulation mechanism, in which a total downregulation of mGluR1 is compensated by an upregulation of mGluR1 on the PM of the dendritic spine. In terms of synaptogenesis, activation of mGluR1 leads to protein kinase-C-γ (PKCγ) activity, and subsequent phosphorylation of calmodulin-dependent protein kinase-2β (CaMKIIβ), which has been shown to repress spine synaptogenesis on PNs [40]. Interestingly, a previous study reported that overstimulation of mGluR1 on cultured hippocampal neurons resulted in prominent dendritic spine elongation into thin spines [41].

Consistent with the changes in dendritic branching and mGluR1 expression in nNOS$^{-/-}$ PNs, vGluT1 expression in PFs was also lower in nNOS$^{-/-}$ mice at PD7. Interestingly, this deficit in vGluT1 expression was not noticeable in 2W or 7W nNOS$^{-/-}$ mice, suggesting the importance of NO signaling on PF maturation during the early postnatal development period. Accordingly, granule cell migration and PF maturation relies on NO production [42], which may explain the delay in vGluT1 protein expression levels at PD7 in nNOS$^{-/-}$ mice. Our results suggest that NO plays an age-dependent role during development, contributing to PF development in younger ages, while not being the main modulator of PF terminal maintenance into adulthood. This topic concerning the development of PF terminals in relation to NO signaling has not yet been elucidated and warrants further investigation.

In comparison with age-matched WT, the cerebellum of nNOS$^{-/-}$ mice at 7W showed an increase in vGluT2 protein expression, suggestive of increased CF boutons, and therefore more CF-PN synapses. Increased CF-PN innervation can result in motor deficits such as tremor and motor

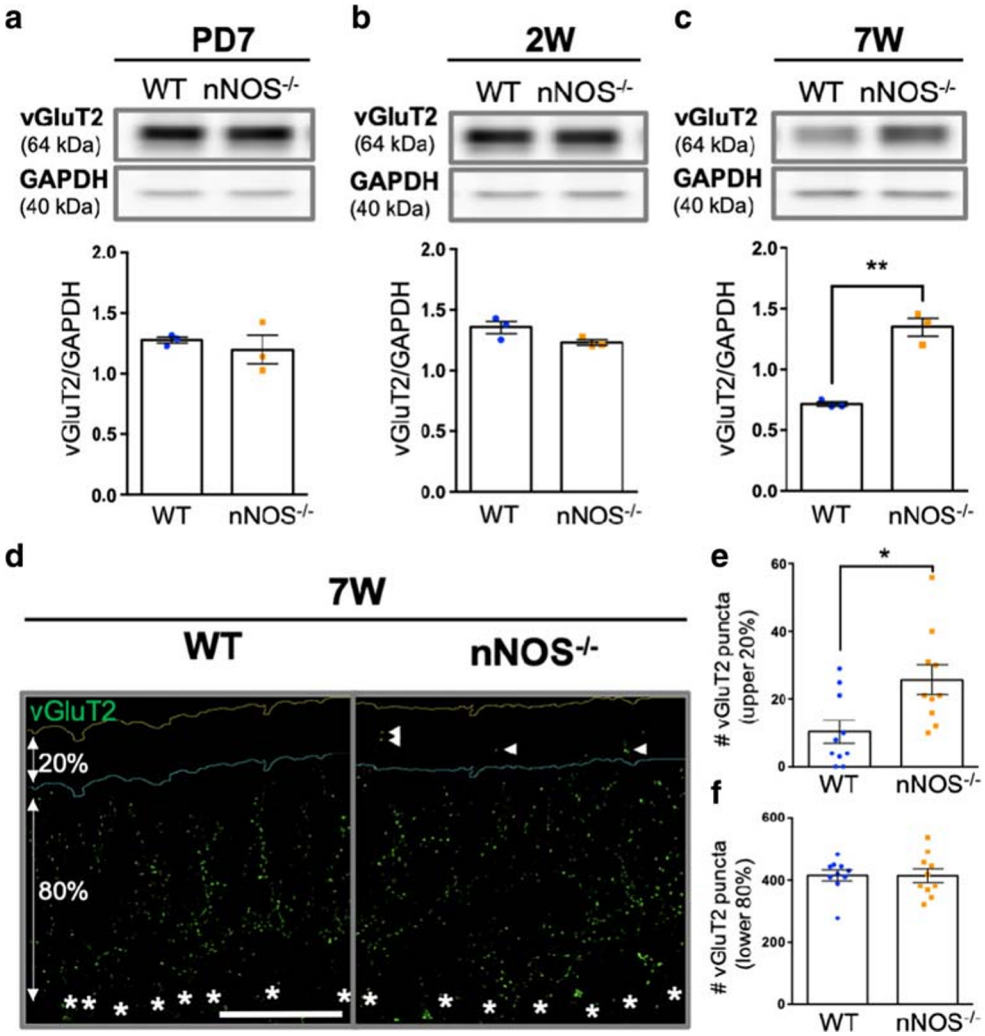

Fig. 6 vGluT2 expression is elevated in 7W nNOS$^{-/-}$ cerebella, but not in PD7 or 2W. **a** Representative western blot of WT and nNOS$^{-/-}$ PD7 cerebellar tissue denoting vGluT2 (64 kDa) expression. Bar graph depicts $N = 3$ biological replicates per group. vGluT2 protein expression was normalized to total GAPDH (40 kDa) protein expression. $P = 0.5433$. **b** Representative western blot of WT and nNOS$^{-/-}$ 2W cerebellar tissue denoting vGluT2 expression. Bar graph depicts $N = 3$ biological replicates per group. $P = 0.0984$. **c** Representative western blot of WT and nNOS$^{-/-}$ 7W cerebellar tissue denoting vGluT2 protein expression. Bar graph depicts $N = 3$ biological replicates per group. vGluT2 protein expression was normalized to GAPDH expression for each sample. $P = 0.0012$. **d** Representative image of 7W WT and nNOS$^{-/-}$ CF synapses visualized by vGluT2 (green). Yellow line denotes edge of the molecular layer. Blue line denoted border between upper 20% and lower 80% of the molecular layer. White asterisks represent PN cell somata. Scale bar represents 50 μm. **e** Bar graph depicts total number of vGluT2 clusters localized within the upper 20% of the molecular layer per image analyzed. $N = 4$ biological replicates per group; WT $n = 10$ images, nNOS$^{-/-}$ $n = 10$ images. $P = 0.0134$. **f** Bar graph depicts total number of vGluT2 clusters localized within the lower 80% of the molecular layer per image. $N = 4$ biological replicates per group; WT $n = 10$ images, nNOS$^{-/-}$ $n = 10$ images. $P = 0.9658$. All data are represented as mean ± SEM

dyscoordination, both in animal models and in a clinical setting [43–45]. Given that increases in vGluT2 were only apparent at 7W and not at PD7 or 2W, the late phase of CF synapse elimination is most likely to be impaired in nNOS$^{-/-}$ mice [46]. Elimination of weak CF synapses in the late phase is governed by mGluR1-mediated PKCγ activation [47, 48]. Specifically, in mice lacking either mGluR1 or PKCγ protein expression, CF elimination is significantly impaired [47, 49]. Moreover, mGluR1-deficient mice result in a PN morphology similar to the nNOS$^{-/-}$ PN morphology reported in our study [47]. However, according to Kano et al., dendritic morphology does not necessarily dictate the amount of CF innervation, while mGluR1/PKC seems to be the predominant influence [47]. Therefore, increased CF innervation within nNOS$^{-/-}$ mice may be attributed to the total decreases in mGluR1 expression noted in nNOS$^{-/-}$ mice, rather than thicker PN branches, as reported within this study. In addition, increases in vGluT2 seem to arise from the infiltration of vGluT2 clusters into the upper 20% of the molecular layer—a largely PF-dominated area [50]. Numerous articles have reported the consequences of extensive CF innervation, which can be found in disorders such as essential tremor in humans

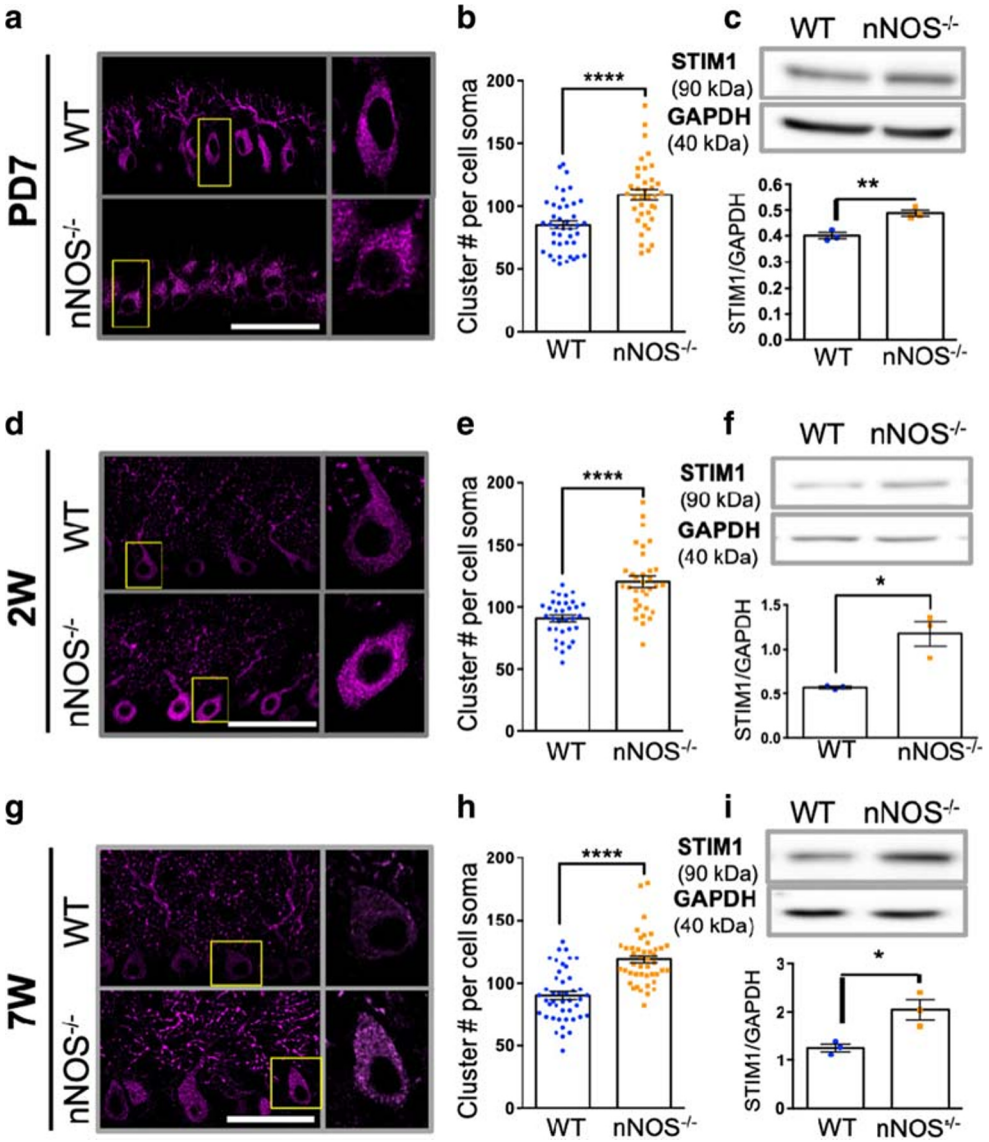

Fig. 7 STIM1 expression is increased in PD7, 2W, and 7W nNOS$^{-/-}$ cerebella. **a** Representative confocal images of PD7 WT and nNOS$^{-/-}$ PNs that show STIM1 (magenta) localization. Scale bar represents 50 μm. **b** Bar graph represents number of STIM1 clusters per PN soma at PD7. $N = 4$ biological replicates per group; WT $n = 42$ cells, nNOS$^{-/-}$ $n = 37$ cells. $P < 0.0001$. **c** Representative western blot of STIM1 (90 kDa) protein expression of WT and nNOS$^{-/-}$ cerebellar tissue at PD7. STIM1 protein expression was normalized to GAPDH (40 kDa). Bar graph represents $N = 3$ biological replicates per group. $P = 0.0065$. **d** Representative confocal images of 2W WT and nNOS$^{-/-}$ PNs that show STIM1 (magenta) localization. Scale bar represents 50 μm. **e** Bar graph represents number of STIM1 clusters per PN soma at 2W. $N = 4$ biological replicates per group; WT $n = 34$ cells, nNOS$^{-/-}$ $n = 33$ cells. $P < 0.0001$. **f** Representative western bot of STIM1 protein expression of WT and nNOS$^{-/-}$ cerebellar tissue at 2W. STIM1 protein expression was normalized to GAPDH. Bar graph represents $N = 3$ biological replicates per group. $P = 0.0129$. **g** Representative confocal images of 7W WT and nNOS$^{-/-}$ PNs that show STIM1 (magenta) localization. Scale bar represents 50 μm. **h** Bar graph represents number of STIM1 clusters per PN soma at 7W. $N = 4$ biological replicates per group; WT $n = 44$ cells, nNOS$^{-/-}$ $n = 44$ cells. $P < 0.0001$. **f** Representative western blot of STIM1 protein expression of WT and nNOS$^{-/-}$ cerebellar tissue at 7W. STIM1 protein expression was normalized to GAPDH expression. Bar graph represents $N = 3$ biological replicates per group. $P = 0.0229$. All data are represented as mean ± SEM

[50], and have related excessive or mislocalized CF innervation with altered calcium homeostasis, leading to excitotoxicity [51, 52].

Along with the increased PM expression of mGluR1 in nNOS$^{-/-}$ mice, significant increases in STIM1 protein expression and clustering were found at PD7, 2W, and 7W. It is known that following mGluR1 activation, STIM1 proteins oligomerize and control store-operated calcium entry through TRPC3 channels [14, 15]. Therefore, changes in expression levels and oligomerization patterns of STIM1 are indicative of calcium dysregulation [53]. Our results displayed increased STIM1 clustering in nNOS$^{-/-}$ PNs, alluding to aberrant calcium entry through a store-operated calcium entry mechanism. Indeed, a recent study noted the interaction between STIM1

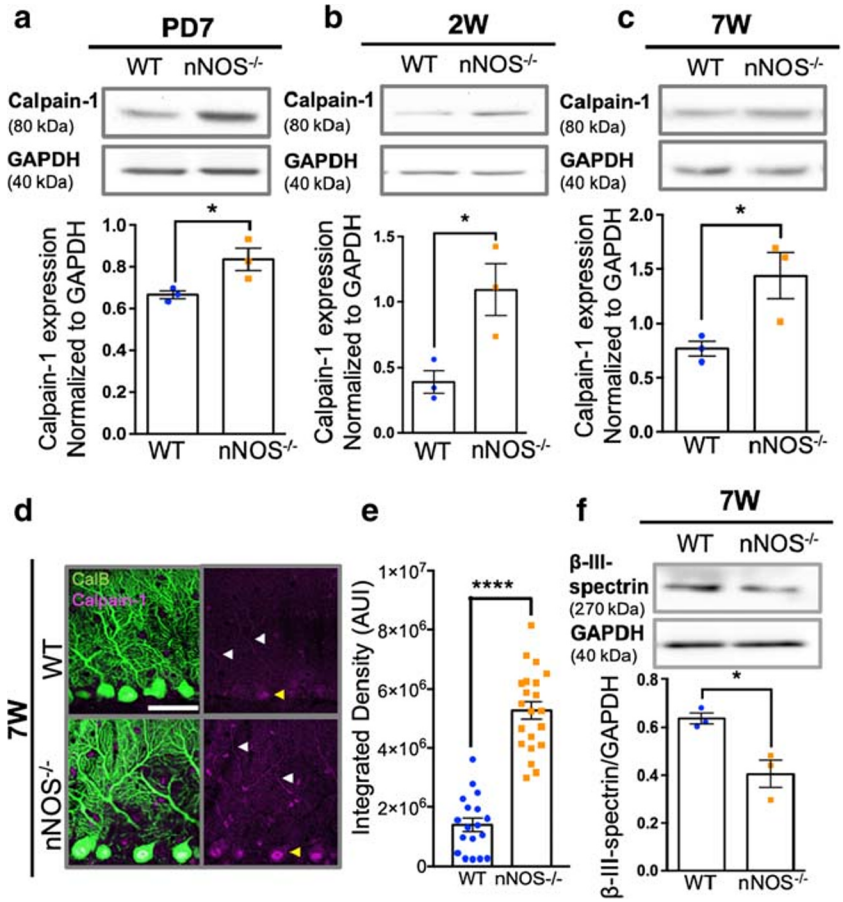

Fig. 8 Calpain-1 protein expression is upregulated, while β-III-spectrin is downregulated in nNOS$^{-/-}$ cerebella. **a** Representative western blot depicting protein expression of calpain-1 (80 kDa) in PD7 WT and nNOS$^{-/-}$ cerebella, along with bar graph representing $N = 3$ biological replicates per group. Calpain-1 protein bands were normalized to total GAPDH (40 kDa) expression. $P = 0.0436$. **b** Representative western blot showing calpain-1 expression in 2W WT and nNOS$^{-/-}$ cerebellar tissue, along with bar graph representing $N = 3$ biological replicates per group. Calpain-1 protein was normalized to GAPDH expression. $P = 0.0351$. **c** Representative western blot depicting calpain-1 protein expression in 7W WT and nNOS$^{-/-}$ cerebella, along with bar graph representing $N = 3$ biological replicates per group. Calpain-1 bands were normalized to total GAPDH expression. $P = 0.0398$. **d** Representative confocal images of 7W WT and nNOS$^{-/-}$ PNs that show calpain-1 (magenta) localization, along with an overlay of Calb (green). Scale bar represents 50 μm. White arrowheads point to PN dendritic localization of calpain-1, while yellow arrowheads point to PN soma localization of calpain-1. **e** Bar graph depicting calpain-1 integrated density represented as arbitrary units of intensity (AUIs) of the fluorescence images in 7W WT and nNOS$^{-/-}$ PN somata, representing $N = 4$ biological replicates per group; WT $n =$ 18 cells, nNOS$^{-/-}$ $n = 21$ cells. $P < 0.0001$. **f** Representative western blot depicting expression of β-III-spectrin (270 kDa) in 7W WT and nNOS$^{-/-}$ cerebella, along with bar graph representing $N = 3$ biological replicates per group. Expression of β-III-spectrin was normalized to total GAPDH expression. $P = 0.0193$. All data are represented as mean ± SEM

and NO via *S*-nitrosylation, resulting in the prevention of STIM1 oligomerization and further reduction of store-operated calcium entry [18]. The absence of NO/*S*-nitrosylation of STIM1 may result in elevated calcium entry through STIM1-gated TRPC3 channels in PNs, initiated by increased PM expression of mGluR1 in nNOS$^{-/-}$ mice.

Calpain-1 Is Increased in the PNs of nNOS$^{-/-}$ Mice

Considering the importance of STIM1 as a regulator of intracellular calcium, we assessed the potential outcome of dysregulated calcium influx by measuring calpain-1 in the cerebellum of WT and nNOS$^{-/-}$ mice. As calcium-dependent cysteine proteases, calpains in neuronal cells are crucial for the regulation of synaptic plasticity, morphology, and neurodegeneration [54]. Calpain activity can induce degradation of neuronal cytoskeletal proteins [55, 56], including α- and β-spectrins [57] as well as IP3 receptors [58], implicated in the progression of multiple SCAs [59–61]. Results from immunohistochemical assays showed that calpain-1 was globally expressed in cells of the cerebellar cortex, with a particularly higher expression within PN somata and dendrites. Notably, we revealed a significant increase in calpain-1 expression across all time points using western blotting, along with a decrease in β-III-spectrin expression in adult nNOS$^{-/-}$ mice. β-III-Spectrin is crucial in regulating glutamate transport on

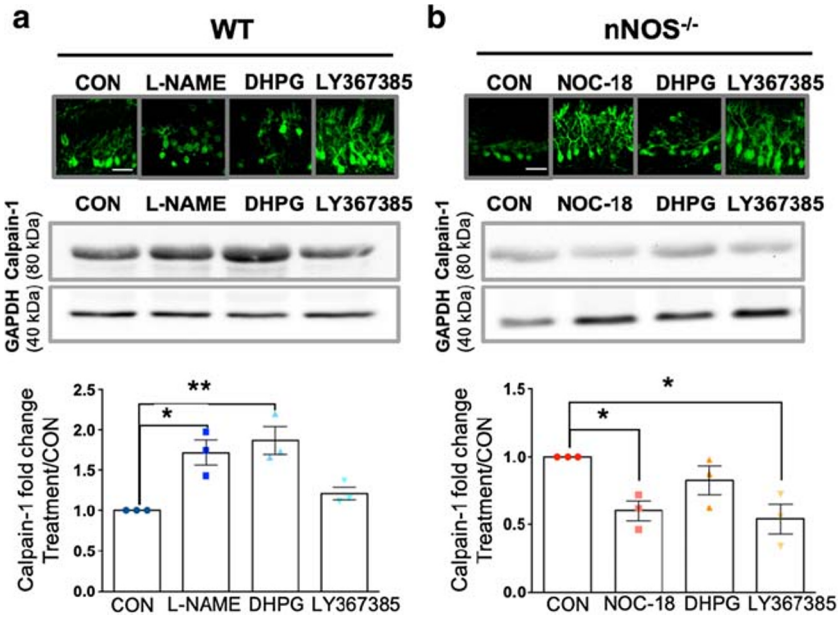

Fig. 9 mGluR1-mediated expression of calpain-1 expression is modulated by NO signaling in ex vivo organotypic cerebellar slice cultures. **a** Representative confocal images of WT DIV7 ex vivo organotypic cerebellar slice cultures treated with L-NAME, DHPG, or LY367385 and stained with CalB (green). Scale bar represents 50 μm. **b** Representative western blot of calpain-1 (80 kDa) expression in WT slices treated with L-NAME (100 μM), DHPG (10 μM), or LY367385 (10 μM). Calpain-1 expression was normalized to GAPDH (40 kDa). Bar graph represents $N = 3$ experimental replicates. Each replicate used $n =$ 10–12 WT pups. $F(3, 8) = 11.36$, $P = 0.003$, ANOVA. **c** Representative confocal images of nNOS$^{-/-}$ DIV7 ex vivo organotypic slice cultures treated with NOC-18, DHPG, or LY367385 and stained with CalB (green). Scale bar represents 50 μm. **d** Representative western blot of calpain-1 expression in nNOS$^{-/-}$ slices treated with NOC-18 (300 μM), DHPG (10 μM), or LY367385 (10 μM). Calpain-1 expression was normalized to total GAPDH. Bar graph represents $N = 3$ experimental replicates. Each replicate used $n = 10$–12 nNOS$^{-/-}$ pups. $F(3, 8) = 6.212$, $P = 0.0174$, ANOVA. All data are represented as mean ± SEM

PNs and is consequently implicated in SCA5 [59, 62]. Given that β-III-spectrin is necessary for the formation of mushroom-like dendritic spines [63], the reduction of β-III-spectrin in the cerebellum may explain the alterations in dendritic structures and synapses in nNOS$^{-/-}$ PNs.

NO Supplementation Can Rectify Deficits in Ex Vivo nNOS$^{-/-}$ Cerebella

Results from ex vivo experiments in this study showed that modulation of NO signaling significantly altered calpain-1 protein expression in both WT and nNOS$^{-/-}$ cerebellar slices. Specifically, inhibition of endogenous NOS activity by L-NAME appeared to hinder PN dendritic branching and significantly increased calpain-1 expression in WT cerebellar tissues. The L-NAME treatment was similar to the effect of DHPG on WT slices, known to cause elevated calcium levels and PN dendritic deficits in previous studies [64, 65], as well as affect calpain-1 expression and activity [66]. Accordingly, NOC-18 and LY367385 mitigated the appearance of PN dendritic deficits and decreased the levels of calpain-1 in nNOS$^{-/-}$ cerebellar slices. These results indicate a critical role for NO signaling in the regulation of PN morphology and function by decreasing calpain-1 levels within the cerebellum.

It is important to note that mGluR1 blockade alone in nNOS$^{-/-}$ slices significantly decreased levels of calpain-1 expression, while activation of mGluR1 showed no significant differences in calpain-1 expression compared with the control. These results suggest that basal mGluR1 activity is upregulated in nNOS$^{-/-}$ cerebella, likely due to increased PM mGluR1 expression on the PNs of nNOS$^{-/-}$ mice. Although nNOS$^{-/-}$ cerebella displayed decreased total mGluR1 expression in vivo, vGluT1 expression remained similar, while vGluT2 expression significantly increased. This imbalance of presynaptic and postsynaptic compartments in vivo may result in an overload of glutamate within PF-PN and CF-PN synaptic clefts, leading to further overexcitation of mGluR1 receptors and overload of intracellular calcium of PNs in NOS$^{-/-}$ cerebella. Characterization of this potential excitotoxic effect should be considered for future studies.

In summary, results from this study indicate that nNOS/NO signaling critically controls PN morphological development by regulating mGluR1 signaling. As depicted in Fig. 10, mGluR1 activation causes ER calcium efflux, STIM1 oligomerization, and consequently calcium entry through STIM1-

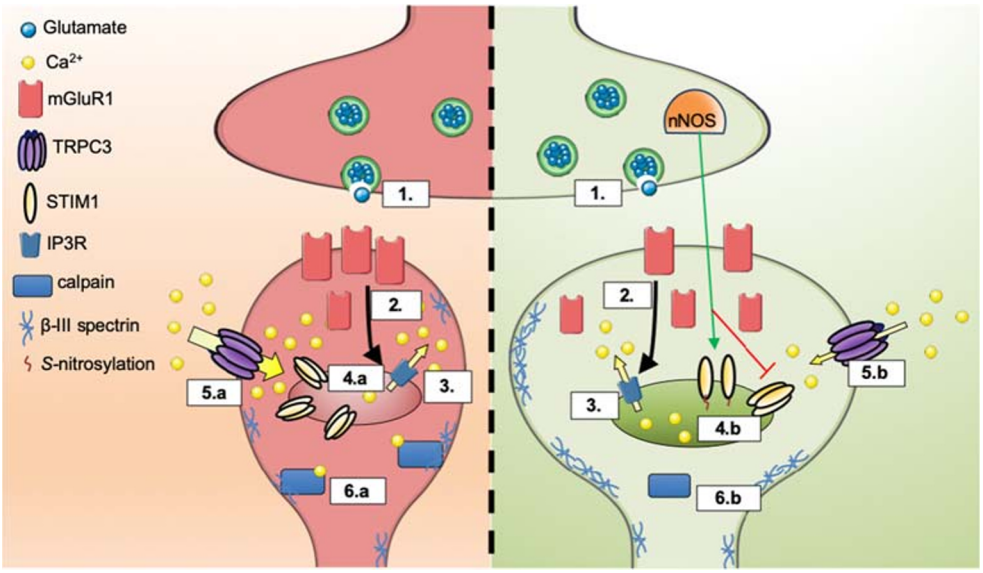

Fig. 10 Schematic representation of the mGluR1 signaling cascade in relation to NO signaling. The left side of this figure depicts a glutamatergic PN synapse in the absence of nNOS-derived NO signaling, while the right depicts a physiological glutamatergic PN synapse with nNOS expression and NO production. (1) Glutamate is released from the presynaptic terminal and binds to mGluR1 receptors on PN dendritic spines. (2) Through a G_q signaling cascade, mGluR1 activation stimulates the production of IP3 in PNs, leading to activation of the IP3R on the ER. (3) IP3R activation causes a calcium efflux from internal ER stores to the PN cytosol. *Left side (nNOS$^{-/-}$)* (4.a) Excessive mGluR1 activation results in ER calcium depletion and causing STIM1 oligomerization. (5.a) Chronically oligomerized STIM1 proteins interact and gate the opening of TRPC3 channels on the PN membrane, causing elevated calcium influx into the PN cytosol. (6.a) Chronically elevated calcium levels within the PN activates calcium-dependent proteases such as calpain-1, which cleaves integral structural proteins such as β-III-spectrin, leading to changes in PN dendritic morphology. *Right side (WT)*: (4.b) NO release from the presynaptic terminal induces *S*-nitrosylation of STIM1, restricting its oligomerization and limiting calcium entry through TRPC3 channels. (5.b) Limited calcium entry through TRPC3 channels replenishes ER calcium stores. (6.b) Physiological concentrations of intracellular calcium controls calpain-1 protease activity, therefore maintaining the integrity of PN dendritic spines

gated TRPC channels [14, 15]. We propose that under physiological conditions, nNOS/NO signaling maintains calcium homeostasis within PNs by attenuating mGluR1-mediated calcium influx [18]. In contrast, the lack of NO signaling in nNOS$^{-/-}$ mice results in overactivation of mGluR1 leading to elevated expression of calcium-dependent proteases such as calpains, increasing degradation of structural proteins such as β-III-spectrin, and resulting in PN structural malformations. Further analysis of the PN phenotype in nNOS$^{-/-}$ mice will provide novel insight into the role of NO signaling in PN development and morphogenesis, along with a potential new mechanism and model of cerebellar ataxia.

Acknowledgments This work was supported by the Canadian Institutes of Health Research (MOP-133504) awarded to W-Y L. VT, and MJEM were awarded Ontario Graduate Scholarships.

Compliance with Ethical Standards

Conflict of Interest The authors declare that they have no competing interests.

Ethics Statement All procedures performed in studies involving animals were in accordance with the ethical standards of the Animal Care and Veterinary Services at the University of Western Ontario under the Animal Use Protocol (#2018-106).

References

1. Blanco S, Molina FJ, Castro L, Del Moral ML, Hernandez R, Jimenez A, et al. Study of the nitric oxide system in the rat cerebellum during aging. BMC Neurosci. 2010 [cited 2019 May 28];11(1):78. Available from: http://www.biomedcentral.com/1471-2202/11/78.
2. Daniel H, Levenes C, Crépel F. Cellular mechanisms of cerebellar LTD. Trends Neurosci. 1998;21(9):401–7.
3. Abbott L, Nahm S. Neuronal nitric oxide synthase expression in cerebellar mutant mice. Cerebellum. 2004;3(3):141–51. Available from: https://doi.org/10.1080/14734220410031927.
4. Kriegsfeld LJ, Eliasson MJ, Demas GE, Blackshaw S, Dawson TM, Nelson RJ, et al. Nocturnal motor coordination deficits in neuronal nitric oxide synthase knock-out mice. Neuroscience. 1999;89(2):311–5. Available from: http://www.ncbi.nlm.nih.gov/pubmed/10077313.
5. Nelson R, Demas G, Huang P, Fishman M, Dawson V, Dawson T, et al. Behavioural abnormalities in male mice lacking neuronal nitric oxide synthase. Nature. 1995;378(6555):383–6. Available from: http://www.ncbi.nlm.nih.gov/pubmed/7477374.
6. Huang PL, Dawson TM, Bredt DS, Snyder SH, Fishman MC. Targeted disruption of the neuronal nitric oxide synthase gene. Cell. 1993;75:1273–86.
7. Lev-Ram V, Makings LR, Keitz PF, Kao JPY, Tsien RY. Long-term depression in cerebellar Purkinje neurons results from coincidence of nitric oxide and depolarization-induced Ca2+ transients. Neuron. 1995 [cited 2019 May 28];15(2):407–15. Available from: https://linkinghub.elsevier.com/retrieve/pii/0896627395900446.

8. Kasumu A, Bezprozvanny I. Deranged calcium signaling in Purkinje cells and pathogenesis in spinocerebellar ataxia 2 (SCA2) and other ataxias. Cerebellum. 2012 [cited 2019 May 28];11(3):630–9. Available from: https://doi.org/10.1007/s12311-010-0182-9.
9. Toru S, Murakoshi T, Ishikawa K, Saegusa H, Fujigasaki H, Uchihara T, et al. Spinocerebellar ataxia type 6 mutation alters P-type calcium channel function. J Biol Chem. 2000 [cited 2019 May 28];275(15):10893–8. Available from: http://www.jbc.org/.
10. Liu J, Tang T-S, Tu H, Nelson O, Herndon E, Huynh DP, et al. Deranged calcium signaling and neurodegeneration in spinocerebellar ataxia type 2. J Neurosci. 2009 [cited 2019 May 28];29(29):9148–62. Available from: http://www.jneurosci.org/content/jneuro/29/29/9148.full.pdf.
11. Hartmann J, Henning HA, Konnerth A. mGluR1/TRPC3-mediated synaptic transmission and calcium signaling in mammalian central neurons. Cold Spring Harb Perspect Biol. 2011;3(4):1–16.
12. Jin Y, Kim SJ, Kim J, Worley PF, Linden DJ. Long-term depression of mGluR1 Signaling. Neuron. 2007;55(2):277–87.
13. Willard SS, Koochekpour S. Glutamate, glutamate receptors, and downstream signaling pathways. Int J Biol Sci. 2013;9(9):948–59.
14. Hartmann J, Dragicevic E, Adelsberger H, Henning HA, Sumser M, Abramowitz J, et al. TRPC3 channels are required for synaptic transmission and motor coordination. Neuron. 2008 [cited 2019 Jul 16];59(3):392–8. Available from: https://www.sciencedirect.com/science/article/pii/S0896627308005023?via%3Dihub.
15. Hartmann J, Karl RM, Alexander RPD, Adelsberger H, Brill MS, Rühlmann C, et al. STIM1 controls neuronal Ca2+ signaling, mGluR1-dependent synaptic transmission, and cerebellar motor behavior. Neuron. 2014 [cited 2019 Jun 3];82(3):635–44. Available from: https://www.sciencedirect.com/science/article/pii/S0896627314002578.
16. Schilling K, Schmidt HH, Baader SL. Nitric oxide synthase expression reveals compartments of cerebellar granule cells and suggests a role for mossy fibers in their development. Neuroscience. 1994;59(4):893–903.
17. Yoshida T, Inoue R, Morii T, Takahashi N, Yamamoto S, Hara Y, et al. Nitric oxide activates TRP channels by cysteine S-nitrosylation. Nat Chem Biol. 2006;2(11):596–607.
18. Gui L, Zhu J, Lu X, Sims SM, Lu W-Y, Stathopulos PB, et al. S-Nitrosylation of STIM1 by neuronal nitric oxide synthase inhibits store-operated Ca2+ entry. J Mol Biol. 2018.
19. Power EM, Morales A, Empson RM. Prolonged type 1 metabotropic glutamate receptor dependent synaptic signaling contributes to spino-cerebellar ataxia type 1. J Neurosci. 2016;36(18):4910–6. Available from: https://doi.org/10.1523/JNEUROSCI.3953-15.2016.
20. Conquet F, Bashir ZI, Davies CH, Daniel H, Ferraguti F, Bordi F, et al. Motor deficit and impairment of synaptic plasticity in mice lacking mGluR1. Nature. 1994 [cited 2019 May 28];372(6503):237–43. Available from: http://www.nature.com/articles/372237a0.
21. Fogel BL, Hanson SM, Becker EBE. Do mutations in the murine ataxia gene TRPC3 cause cerebellar ataxia in humans? Mov Disord. 2015 [cited 2019 May 28];30(2):284–6. Available from: http://www.ncbi.nlm.nih.gov/pubmed/25477146.
22. Rossi PIA, Vaccari CM, Terracciano A, Doria-Lamba L, Facchinetti S, Priolo M, et al. The metabotropic glutamate receptor 1, GRM1: evaluation as a candidate gene for inherited forms of cerebellar ataxia. J Neurol. 2010 [cited 2019 May 28];257(4):598–602. Available from: https://doi.org/10.1007/s00415-009-5380-3.
23. van de Leemput J, Chandran J, Knight MA, Holtzclaw LA, Scholz S, Cookson MR, et al. Deletion at ITPR1 underlies ataxia in mice and spinocerebellar ataxia 15 in humans. PLoS Genet. 2007 [cited 2019 May 28];3(6):e108. Available from: https://doi.org/10.1371/journal.pgen.0030108.
24. Schindelin J, Arganda-Carreras I, Frise E, Kaynig V, Longair M, Pietzsch T, et al. Fiji: an open-source platform for biological-image analysis. Nat Methods. 2012 [cited 2019 Jul 5];9(7):676–82. Available from: http://www.nature.com/articles/nmeth.2019.
25. Suzuki K, Hata S, Kawabata Y, Sorimachi H. Structure, activation, and biology of calpain. Diabetes. 2004;53(Supplement 1):S12–8. Available from: https://doi.org/10.2337/diabetes.53.2007.S12.
26. Bal-Price A, Moneer Z, Brown GC. Nitric oxide induces rapid, calcium-dependent release of vesicular glutamate and ATP from cultured rat astrocytes. Glia. 2002;40(3):312–23.
27. Kakizawa S, Yamazawa T, Iino M. Nitric oxide-induced calcium release. Channels. 2013;7(1):1–5. Available from: https://doi.org/10.4161/chan.22555.
28. Wang D-J, Su L-D, Wang Y-N, Yang D, Sun C-L, Zhou L, et al. Long-term potentiation at cerebellar parallel fiber-Purkinje cell synapses requires presynaptic and postsynaptic signaling cascades. J Neurosci. 2014;34(6):2355–64. Available from: https://doi.org/10.1523/JNEUROSCI.4064-13.2014.
29. Lev-Ram V, Jiang T, Wood J, Lawrence DS, Tsien RY. Synergies and coincidence requirements between NO, cGMP, and Ca2+ in the induction of cerebellar long-term depression. Neuron. 1997 [cited 2019 Jul 16];18(6):1025–38. Available from: https://www.sciencedirect.com/science/article/pii/S0896627300803402?via%3Dihub.
30. Boxall AR, Garthwaite J. Long-term depression in rat cerebellum requires both NO synthase and NO-sensitive guanylyl cyclase. Eur J Neurosci. 1996 [cited 2019 Jul 16];8(10):2209–12. Available from: https://doi.org/10.1111/j.1460-9568.1996.tb00743.x.
31. Lee KJ, Jung JG, Arii T, Imoto K, Rhyu IJ. Morphological changes in dendritic spines of Purkinje cells associated with motor learning. Neurobiol Learn Mem. 2007 [cited 2019 May 28];88(4):445–50. Available from: https://www.sciencedirect.com/science/article/pii/S1074742707000858.
32. Mattson M, Kater S. Calcium regulation of neurite elongation and growth cone motility. J Neurosci. 1987 [cited 2019 Jul 16];7(12):4034–43. Available from: http://www.ncbi.nlm.nih.gov/pubmed/3121806.
33. Mahmmoud RR, Sase S, Aher YD, Sase A, Gröger M, Mokhtar M, et al. Spatial and working memory is linked to spine density and mushroom spines. Chapouthier G, editor. PLoS One. 2015 [cited 2019 May 28];10(10):e0139739. Available from: https://doi.org/10.1371/journal.pone.0139739.
34. Bourne J, Harris KM. Do thin spines learn to be mushroom spines that remember? Curr Opin Neurobiol. 2007;17(3):381–6. Available from: https://linkinghub.elsevier.com/retrieve/pii/S0959438807000633.
35. Dumitriu D, Hao J, Hara Y, Kaufmann J, Janssen WGM, Lou W, et al. Selective changes in thin spine density and morphology in monkey prefrontal cortex correlate with aging-related cognitive impairment. J Neurosci. 2010 [cited 2019 May 28];30(22):7507–15. Available from: http://www.jneurosci.org/content/jneuro/30/22/7507.full.pdf.
36. Coesmans M, Sillevis Smitt PA, Linden DJ, Shigemoto R, Hirano T, Yamakawa Y, et al. Mechanisms underlying cerebellar motor deficits due to mGluR1-autoantibodies. Ann Neurol. 2003 [cited 2019 Jun 3];53(3):325–36. Available from: https://doi.org/10.1002/ana.10451.
37. Kishimoto Y, Fujimichi R, Araishi K, Kawahara S, Kano M, Aiba A, et al. mGluR1 in cerebellar Purkinje cells is required for normal association of temporally contiguous stimuli in classical conditioning. Eur J Neurosci. 2002 [cited 2019 Jun 3];16(12):2416–24. Available from: https://doi.org/10.1046/j.1460-9568.2002.02407.x.
38. Ganeshina O, Berry RW, Petralia RS, Nicholson DA, Geinisman Y. Synapses with a segmented, completely partitioned postsynaptic density express more AMPA receptors than other axospinous synaptic junctions. Neuroscience. 2004 [cited 2019 Jun 3];125(3):615–

23. Available from: https://www.sciencedirect.com/science/article/pii/S0306452204001575.
39. Santamaria F, Wils S, De Schutter E, Augustine GJ. Anomalous diffusion in Purkinje cell dendrites caused by spines. Neuron. 2006 [cited 2019 Jun 3];52(4):635–48. Available from: https://www.sciencedirect.com/science/article/pii/S0896627306008245.
40. Sugawara T, Hisatsune C, Miyamoto H, Ogawa N, Mikoshiba K. Regulation of spinogenesis in mature Purkinje cells via mGluR/PKC-mediated phosphorylation of CaMKIIβ. Proc Natl Acad Sci U S A. 2017 [cited 2019 Jun 3];114(26):E5256–65. Available from: http://www.ncbi.nlm.nih.gov/pubmed/28607044.
41. Vanderklish PW, Edelman GM. Dendritic spines elongate after stimulation of group 1 metabotropic glutamate receptors in cultured hippocampal neurons. Proc Natl Acad Sci. 2002 [cited 2019 Jun 3];99(3):1639–44. Available from: https://doi.org/10.1073/pnas.032681099.
42. Tanaka M, Yoshida S, Yano M, Hanaoka F. Roles of endogenous nitric oxide in cerebellar cortical development in slice cultures. Neuroreport. 1994;5(16):2049–52. Available from: http://www.ncbi.nlm.nih.gov/pubmed/7865742.
43. Pan M-K, Ni C-L, Wu Y-C, Li Y-S, Kuo S-H. Animal models of tremor: relevance to human tremor disorders. Tremor Other Hyperkinet Mov (N Y). 2018 [cited 2019 Jul 16];8:587. Available from: http://www.ncbi.nlm.nih.gov/pubmed/30402338.
44. Kuo S-H, Lin C-Y, Wang J, Sims PA, Pan M-K, Liou J-Y, et al. Climbing fiber-Purkinje cell synaptic pathology in tremor and cerebellar degenerative diseases. Acta Neuropathol. 2017 [cited 2019 Jul 16];133(1):121–38. Available from: http://www.ncbi.nlm.nih.gov/pubmed/27704282.
45. Smeets CJLM, Verbeek DS. Climbing fibers in spinocerebellar ataxia: a mechanism for the loss of motor control. Neurobiol Dis. 2016 [cited 2019 Jul 16];88:96–106. Available from: https://www.sciencedirect.com/science/article/pii/S0969996116300092?via%3Dihub.
46. Kano M, Watanabe T, Uesaka N, Watanabe M. Multiple phases of climbing fiber synapse elimination in the developing cerebellum. The Cerebellum. 2018 [cited 2019 Jun 30];17(6):722–34. Available from: https://doi.org/10.1007/s12311-018-0964-z.
47. Kano M, Hashimoto K, Kurihara H, Watanabe M, Inoue Y, Aiba A, et al. Persistent multiple climbing fiber innervations of cerebellar Purkinje cells in mice lacking mGluR1. Neuron. 1997 [cited 2019 Jun 3];18(1):71–9. Available from: https://www.sciencedirect.com/science/article/pii/S0896627301800477.
48. Offermanns S, Hashimoto K, Watanabe M, Sun W, Kurihara H, Thompson RF, et al. Impaired motor coordination and persistent multiple climbing fiber innervation of cerebellar Purkinje cells in mice lacking G q. Proc Natl Acad Sci. 1997 [cited 2019 Jun 3];94(25):14089–94. Available from: www.pnas.org.
49. Kano M, Hashimoto K, Chen C, Abeliovich A, Aiba A, Kurihara H, et al. Impaired synapse elimination during cerebellar development in PKCγ mutant mice. Cell. 1995 [cited 2019 Jul 16];83(7):1223–31. Available from: https://www.sciencedirect.com/science/article/pii/0092867495901477?via%3Dihub.
50. Lin CY, Louis ED, Faust PL, Koeppen AH, Vonsattel JPG, Kuo SH. Abnormal climbing fibre-Purkinje cell synaptic connections in the essential tremor cerebellum. Brain. 2014 [cited 2019 Oct 2];137(12):3149–59. Available from: https://doi.org/10.1093/brain/awu281.
51. Hashimoto K, Ichikawa R, Takechi H, Inoue Y, Aiba A, Sakimura K, et al. Roles of glutamate receptor δ2 subunit (GluRδ2) and metabotropic glutamate receptor subtype 1 (mGluR1) in climbing fiber synapse elimination during postnatal cerebellar development. J Neurosci. 2001 [cited 2019 Oct 2];21(24):9701–12. Available from: https://www.jneurosci.org/content/jneuro/21/24/9701.full.pdf.
52. Slemmer JE, De Zeeuw CI, Weber JT. Don't get too excited: mechanisms of glutamate-mediated Purkinje cell death. Prog Brain Res. 2005 [cited 2019 Oct 2];148:367–90. Available from: https://www.sciencedirect.com/science/article/pii/S0079612304480297.
53. Klejman ME, Gruszczynska-Biegala J, Skibinska-Kijek A, Wisniewska MB, Misztal K, Blazejczyk M, et al. Expression of STIM1 in brain and puncta-like co-localization of STIM1 and ORAI1 upon depletion of Ca2+ store in neurons. Neurochem Int. 2009 [cited 2019 Jun 3];54(1):49–55. Available from: https://www.sciencedirect.com/science/article/pii/S0197018608001666.
54. Sorimachi H, Ishiura S, Suzuki K. Structure and physiological function of calpains. Biochem J. 1997 [cited 2019 Jun 3];328(3):721–32. Available from: http://www.biochemj.org/content/ppbiochemj/328/3/721.full.pdf.
55. Schumacher PA, Siman RG, Fehlings MG. Pretreatment with calpain inhibitor CEP-4143 inhibits calpain I activation and cytoskeletal degradation, improves neurological function, and enhances axonal survival after traumatic spinal cord injury. J Neurochem. 2002 [cited 2019 Jun 3];74(4):1646–55. Available from: https://doi.org/10.1046/j.1471-4159.2000.0741646.x.
56. Rami A, Ferger D, Krieglstein J. Blockade of calpain proteolytic activity rescues neurons from glutamate excitotoxicity. Neurosci Res. 1997 [cited 2019 Jun 3];27(1):93–7. Available from: https://www.sciencedirect.com/science/article/pii/S0168010296011236.
57. Löfvenberg L, Backman L. Calpain-induced proteolysis of β-spectrins. FEBS Lett. 1999 [cited 2019 Jun 3];443(2):89–92. Available from: https://doi.org/10.1016/S0014-5793%2898%2901697-4.
58. Vosler PS, Brennan CS, Chen J. Calpain-mediated signaling mechanisms in neuronal injury and neurodegeneration. Mol Neurobiol. 2008 [cited 2019 Jun 3];38(1):78–100. Available from: https://doi.org/10.1007/s12035-008-8036-x.
59. Avery AW, Thomas DD, Hays TS. β-III-spectrin spinocerebellar ataxia type 5 mutation reveals a dominant cytoskeletal mechanism that underlies dendritic arborization. Proc Natl Acad Sci U S A. 2017 [cited 2019 Jun 3];114(44):E9376–85. Available from: http://www.ncbi.nlm.nih.gov/pubmed/29078305.
60. Tada M, Nishizawa M, Onodera O. Roles of inositol 1,4,5-trisphosphate receptors in spinocerebellar ataxias. Neurochem Int. 2016 [cited 2019 Jun 3];94:1–8. Available from: https://www.sciencedirect.com/science/article/pii/S0197018616300079?via%3Dihub.
61. Hubener J, Weber JJ, Richter C, Honold L, Weiss A, Murad F, et al. Calpain-mediated ataxin-3 cleavage in the molecular pathogenesis of spinocerebellar ataxia type 3 (SCA3). Hum Mol Genet. 2013 [cited 2019 Jun 3];22(3):508–18. Available from: https://doi.org/10.1093/hmg/dds449.
62. Gao Y, Perkins EM, Clarkson YL, Tobia S, Lyndon AR, Jackson M, et al. β-III spectrin is critical for development of Purkinje cell dendritic tree and spine morphogenesis. J Neurosci. 2011 [cited 2019 Jun 3];31(46):16581–90. Available from: http://www.jneurosci.org/content/31/46/16581?ijkey=933e5b64ae637b2664348b6e6bdf9dee05ac0b2d&keytype2=tf_ipsecsha.
63. Efimova N, Korobova F, Stankewich MC, Moberly AH, Stolz DB, Wang J, et al. βIII Spectrin is necessary for formation of the constricted neck of dendritic spines and regulation of synaptic activity in neurons. J Neurosci. 2017 [cited 2019 Jul 16];37(27):6442–59. Available from: http://www.ncbi.nlm.nih.gov/pubmed/28576936.

64. Hasegawa S, Sakuragi S, Tominaga-Yoshino K, Ogura A. Dendritic spine dynamics leading to spine elimination after repeated inductions of LTD. Sci Rep. 2015;9:5.
65. Sirzen-Zelenskaya A, Zeyse J, Kapfhammer JP. Activation of class I metabotropic glutamate receptors limits dendritic growth of Purkinje cells in organotypic slice cultures. Eur J Neurosci. 2006 [cited 2019 Jun 3];24(11):2978–86. Available from: https://doi.org/10.1111/j.1460-9568.2006.05196.x.
66. Xu W, Wong TP, Chery N, Gaertner T, Wang YT, Baudry M. Calpain-mediated mGluR1α truncation: a key step in Excitotoxicity. Neuron. 2007.